Published in final edited form as:
IEEE Trans Biomed Eng. 2009 November ; 56(11): 2611–2618. doi:10.1109/TBME.2009.2020694.

Comparison of Conventional Filtering and Independent Component Analysis for Artifact Reduction in Simultaneous Gastric EMG and Magnetogastrography From Porcines

Andrei Irimia,
Multimodal Imaging Laboratory, Department of Radiology, University of California at San Diego, La Jolla, CA 92093-0841 USA (irimia@ucsd.edu)

William O. Richards, and
Department of Surgery, Vanderbilt University School of Medicine, Nashville, TN 37235 USA

L. Alan Bradshaw
Departments of Physics and Astronomy and Biomedical Engineering, Vanderbilt University, Nashville, TN 37235 USA

Abstract

In this study, we perform a comparative study of independent component analysis (ICA) and conventional filtering (CF) for the purpose of artifact reduction from simultaneous gastric EMG and magnetogastrography (MGG). EMG/MGG data were acquired from ten anesthetized pigs by obtaining simultaneous recordings using serosal electrodes (EMG) as well as with a superconducting quantum interference device biomagnetometer (MGG). The analysis of MGG waveforms using ICA and CF indicates that ICA is superior to the CF method in its ability to extract respiration and cardiac artifacts from MGG recordings. A signal frequency analysis of ICA- and CF-processed data was also undertaken using waterfall plots, and it was determined that the two methods produce qualitatively comparable results. Through the use of simultaneous EMG/MGG, we were able to demonstrate the accuracy and trustworthiness of our results by comparison and cross-validation within the framework of a porcine model.

Index Terms

Artifact; EMG; filter; independent component analysis (ICA); magnetogastrography (MGG)

I. Introduction

Gastric motility is of interest to clinicians because of the relationship between gastrointestinal (GI) disease and gastric electrical control activity (ECA), which is a sinusoidal signal with a frequency of 3 cycles per minute (cpm) that originates from a pacemaker located in the antral region of the stomach. The interstitial cells of Cajal in this region impose periodic waves of cell membrane depolarization and repolarization that advance along the corpus of the stomach at a rate of 2–4 cpm in men and pigs. Each ECA wave consists of a potential upstroke followed by a plateau, and then by a sustained depolarization phase. A relationship has been established between abnormal ECA and

Correspondence to: Andrei Irimia.

several GI disorders, including gastroparesis, diabetic gastropathy, and gastric myoelectrical dysrhythmia [7].

Three methods used for acquiring ECA recordings are EMG, electrogastrography (EGG), and magnetogastrography (MGG). EMG and EGG involve the use of electrodes that record the bioelectric fields due to ECA. In the case of EMG, electrodes are positioned directly onto the serosa, which makes this technique strictly invasive. In the case of EGG, the electrodes are attached to the abdominal skin. Whereas the SNR of EMG is excellent, that of EGG is extremely poor. For this reason, the reliability of the latter technique has been questioned due to the high dependence of cutaneous electrical recordings upon tissue conductivity, the thickness of the abdominal wall, and the variable propagation velocity of ECA [6]. For human studies, EMG recordings may not be acquired outside the operating room, while EGG recordings have low reliability. Because of this, a third technique has been designed, namely MGG. This consists of the noninvasive acquisition of biomagnetic signals using a superconducting quantum interference device (SQUID) biomagnetometer. The reason for which such an instrument must be used for MGG experiments is because gastric biomagnetic fields are very weak ($O(10^{-12})$ T), and SQUIDs being the only devices that are sensitive enough to record such low-amplitude signals. Because of the disadvantages of EGG/EMG listed before, MGG is a suitable alternative to both EMG and EGG because it involves the noninvasive positioning of a magnetometer in close proximity to the abdomen to detect the biomagnetic field generated by the electric current of ECA. The noninvasive measurement of biomagnetic fields via MGG is more advantageous than the noninvasive measurement of bioelectric fields via EGG because magnetic fields are strongly dependent on tissue permeability, which is nearly equivalent to that of free space. On the other hand, bioelectric fields are dependent primarily upon tissue permittivity, which creates a screening effect between the ECA source and the measurement apparatus in the case of EGG. Because MGG is noninvasive and because its SNR is comparable to that of invasive EMG, magnetic field recordings of ECA can be acquired from human patients with good results even outside the operating room.

One disadvantage of noninvasive ECA recordings, whether electric (EGG) or magnetic (MGG), is the presence of motion, cardiac, and respiratory artifacts. In our previous study [3], we demonstrated the use of independent component analysis (ICA) for the removal of both biological and nonbiological artifacts from multichannel MGG recordings. There, the accuracy of the method was analyzed by comparing ICA-extracted versus electrode-measured respiratory signals to conclude that reliable results could be obtained with MGG in terms of ECA signal extraction. In this study, we describe the use of ICA for signal extraction from simultaneous EMG/MGG recordings rather than from MGG recordings alone. Through the use of this improved technique, we demonstrate the accuracy of our method by not comparing the respiratory signals as in the previous case, but rather the gastric signals themselves. Moreover, we show that ICA is superior to conventional filtering (CF) in its ability to reduce artifacts from MGG recordings.

II. Methods

A. Experimental Protocols

Two techniques were used for data acquisition, namely MGG and EMG. The multichannel 637i SQUID biomagnetometer (Tristan Technologies, Inc., San Diego, CA) in the Vanderbilt University GI SQUID Technology (VU-GIST) Laboratory has detection coils located at the bottom of an insulated dewar made of garolite (G10) and aluminum and filled with liquid helium at a temperature of approximately 4 K. The coils are magnetically coupled to the SQUID coils, which convert magnetic flux incident on the detection coils to voltage signals that are amplified, and then acquired at 3 kHz. The detection coils are

arranged in gradiometer format as a horizontal grid with 19 of them recording the Cartesian component of the magnetic field that is normal with respect to the grid plane (B_z). At five of these 19 locations, the other two Cartesian components of the field (B_x and B_y) are also measured. A detailed description of our MGG setup is given in [4].

Our protocol was approved by the Vanderbilt University Institutional Animal Care and Use Committee (VU-IACUC). In our experiments, subjects lie horizontally under the SQUID in a magnetically shielded room (Amuneal Manufacturing Corporation, Philadelphia, PA). The magnetometer is oriented so that the coils measuring the $\hat{\mathbf{x}}$ and $\hat{\mathbf{y}}$ components of the signal (tangential to the body surface) are oriented in the sagittal and horizontal planes, while the coils measuring the $\hat{\mathbf{z}}$ component (normal to the body surface) are oriented in the frontal plane. The electrode equipment employed for EMG data acquisition consisted of 18 pregelled, disposable, pickup/ground electrodes (Rochester Electro-Med, Inc., Tampa, FL) connected to an isolated bioelectric amplifier (James Long Company, Caroga Lake, NY). Twelve electrodes were manually affixed to the skins of ten fasted, anesthetized healthy pigs of approximately 20–25 kg each, which were placed horizontally under the SQUID inside the magnetically shielded room. Initial anaesthesia consisted of intravenous injections of telazol, ketamine, and xylazine, each at a concentration of 100 mg/mL. The dosage administered was 4.4 mg/kg telazol, 2.2 mg/kg ketamine, and 2.2 mg/kg xylazine. The animals were intubated and maintained on isoflurane anaesthesia with a concentration of 2%. Respiration sensors were placed on the mouth and nose of each pig. EMG data were acquired using a personal computer (Dell, Austin, TX) through analog-to-digital conversion boards interfaced with custom LabVIEW software (PCI-6033E, National Instruments, Austin, TX) with a sample frequency of 3 kHz and decimation to 300 Hz. EMG envelope detection was accomplished by low-pass decimation filtering using a high-resolution analog-to-digital converter (ADC, Biosemi Instrumentation, Amsterdam, The Netherlands), which had a fifth-order sinc response with a −3 dB point at one-fifth of the sampling rate. Simultaneous EMG/MGG data were acquired for a duration of 15 min. To investigate and compare the ability of CF and ICA to reduce respiration artifacts from the data, 1-min breathholds were induced twice throughout the recording. The induction of breathholds was done by suspending the artificial respiration that was sustained by the intubator.

B. Analysis Methods

Two data analysis methods were implemented separately for comparison, namely CF and ICA. The CF analysis performed consisted of the application of a bandpass, second-order Butterworth filter. The Butterworth filter is maximally flat in the passband and monotonic overall, which reduces the effect of passband ripples in the signal to a minimum. Butterworth filters sacrifice roll-off steepness in favor of having a magnitude function that changes monotonically with frequency in the passband and stopband. The filtering window used was [1/2, 15] cpm. Data are filtered using the Butterworth filter in the forward and reverse directions for zero-phase filtering. In addition to the forward–reverse filtering, the filtering process attempts to minimize start-up transients by adjusting initial conditions to match the dc component of the signal and by prepending several filter lengths of a flipped, reflected copy of the input signal.

Because our ICA implementation is described in detail in [3], only a brief description is supplied here. ICA is a data analysis technique whose purpose is to solve the so-called blind signal separation (BSS) problem, which consists of recovering unobserved signals or "sources" from observed mixtures, i.e., from the output of an array of sensors [1]. Let x_1, x_2, …, x_n be a set of n observed random variables expressed as linear combinations of another n random variables s_1, s_2,…, s_n, i.e., $x_i = a_{i1}\, s_1 + a_{i2}\, s_2 + \cdots + a_{in}\, s_n = \sum_{j=1}^{n} a_{ij}\, s_j$, where $i = 1, \ldots, n$ and $a_{ij} \in \mathbb{R}$. The variables s_i are assumed to be statistically mutually independent. Let $\mathbf{x}$ and

s be random vectors that contain the mixtures $x_1, x_2,\ldots, x_n$ and $s_1, s_2,\ldots, s_n$, respectively, and let **A** be the matrix with entries $A_{ij} = a_{ij}$. The aforementioned mixing model can then be written as **x** = **As**. The task of ICA is to find **s** (the underlying gastric, cardiac, etc., signals) in terms of given **x** (MGG or EMG signals) by finding **A**. The fixed-point fast ICA (FICA) algorithm of Hyvärinen was used, as described in detail in [2]. Before ICA, however, data sphering as well as dimensionality reduction using principal component analysis (PCA) were both applied to the data. Although PCA was not found to have the ability to separate cardiac or respiration artifacts satisfactorily, it was nevertheless useful in eliminating a limited number of extremely large artifacts. The ICA of **x** is defined as an invertible transformation of the form **s** = **Wx**. The task of ICA is carried out by identifying a suitable choice of the matrix elements of **A**. The resulting estimator of **A** as found by ICA can be denoted by $\hat{\mathbf{A}} = \mathbf{W}^{-1}$, such that the relationship $\mathbf{x} = \hat{\mathbf{A}}\hat{\mathbf{s}}$ is satisfied (a distinction is made here between the true sources **s** and their estimators $\hat{\mathbf{s}}$ obtained via ICA).

After computing the ICs as described before, a set of "ICA-reconstructed" signals was obtained as follows. First, the frequency spectrum was computed for each IC. Then, the energy content percentage, denoted by *c*, within the range of GI activity (1.5–15 cpm) was computed. In the next step, the rows in the matrix **W** that corresponded to ICs with $c \leq 0.15$ (15% or less GI frequency content) were set to zero. After visual inspection of all IC waveforms and their spectrograms, a value of 0.15 was chosen for *c* because it was found that all ICs with $c \leq 0.15$ corresponded to recognizable artifacts such as SQUID hardware resets, movement of large ferromagnetic objects (vehicles, elevator doors, etc.) in the vicinity of the laboratory, etc. The new matrix that was obtained, denoted by **Z**, is similar to the matrix **W** described before, with the difference that **Z** does not contain information pertaining to ICs that contribute little to the GI content of the original signals **x**. After computing $\hat{\mathbf{A}} = \mathbf{W}^{-1}$, one can similarly remove the columns in $\hat{\mathbf{A}}$ corresponding to the unwanted components and obtain a new matrix, denoted by **Y**. By performing the operation $\mathbf{x}' = \mathbf{Y}\,\mathbf{Z}\hat{\mathbf{s}}$, one can obtain a new set of signals $\mathbf{x}'$, which are similar to the original recorded signals **x** but with the difference that no information is included that comes from ICs that have $c \leq 0.15$. In practice, such ICs contain cardiac, respiration, motion, and other similar artifacts whose elimination is, of course, warranted. The matrix product $\mathbf{Z}\,\hat{\mathbf{s}}$ contains what are known as the *activations* at the desired components, while the matrix $\mathbf{x}'$ contains the so-called *projections* of the activations to reconstitute the observed data using only the selected ICs. These ICA-reconstructed signals are the ones based on which the comparison with CF is made in the following section. The motivation for using these reconstructed signals rather than the original ICs is the fact that a *comparison* of CF and ICA was attempted in this study. In our previous undertaking [3], it was, of course, demonstrated that gastric signals can be isolated using ICA, but no comparison of methods was attempted there. To compare ICA and CF fairly, however, it was necessary, for the purpose of this study, to identify a manner of studying the results of the two methods in a similar data format. As a result, the method of ICA-reconstructed signals was used in order to focus on the abilities of the two methods to extract artifacts without introducing any bias in favor of ICA.

III. Results

Our first comparative analysis of waveforms obtained using CF and ICA is presented in Fig. 1. There, simultaneous EMG/MGG data are shown for 1 min of recording time. Two different segments were chosen, namely one acquired during a breathhold (first column) and another acquired during respiration (second column). In the case of raw data acquired during the breathhold (top left), no respiration artifact is visible, as expected. The most easily identifiable artifact in this case is of cardiac origin and has a frequency of about 80 cpm. This artifact is visible only in MGG data (shown using a continuous trace, black color online) while the EMG raw signal (dashed trace, red color online) is not affected by cardiac

activity. The reason for this is the fact that EMG signals are generated primarily by sources in the immediate physical proximity of the sensor, while MGG signals can also be affected by sources that are farther away. Because electrode signals depend to a very large extent on tissue conductivity, electrical sources that are far from the recording site do not contribute to the signal appreciably. In the case of MGG, the quality and strength of the signal are dependent on tissue permeability, which is very nearly equal to that of free space for biological matter. This is why, although SQUID coils are farther from the source than electrodes are during a typical experiment (the latter being affixed directly to the external gastric surface), the MGG signal is more sensitive to cardiac activity than the EMG signal. This situation was encountered in all ten animals that made the subject of this study. The raw data segment acquired during the breathhold (top left) can be compared to the raw data segment acquired during respiration (top right). In the latter, the respiration artifact is clearly visible in the case of MGG at a frequency of about 32 cpm. Generally, the frequency of respiration for each animal was found to be in the range of 27–35 cpm. The cardiac artifact is also present in the figure, though its amplitude is lower. The EMG signal was not found to appreciably affected by respiration in any of the subjects, a finding that is illustrated in the figure as well. This phenomenon is due to the fact that the relative electrode position with respect to the gastric electric source remains unchanged throughout respiration, whereas for MGG, this is not the case. As a result, EMG signal properties remain largely unchanged whether acquired during respiration or during a breathhold.

The second row in Fig. 1 displays the EMG and MGG signals after CF processing. In the case of EMG, results are very similar for breathhold and respiration data. In the case of MGG, large differences exist. First of all, the CF method is not capable of removing the respiration artifact in a satisfactory manner, as shown in the plot in the middle right. In fact, the respiration artifact could not be satisfactorily reduced in any of the subjects in our study. Second, the EMG and MGG processed signals are more strongly correlated during the breathhold than they are during respiration. Across all animals, the correlation coefficient ρ between EMG and MGG signals during breathholds was first converted using the Fisher z' transformation, due to the fact that, as an anonymous reviewer noted, ρ values had been derived from a bounded distribution. The z' statistic was found to have a mean of 0.933 with a standard deviation across subjects of 0.134. The corresponding mean and standard deviation of the z' statistics for data acquired during respiration were 0.124 and 0.089, respectively. The ICA results are shown in the third row of Fig. 1. There, it can be seen that ICA is largely unaffected by the presence of respiration artifacts in the original data. Moreover, the correlation between the EMG and MGG waveforms is higher in both ICA cases as compared to CF-processed data. The Fisher z' statistic across subjects for ICA-processed data had a mean of 0.765 with a standard deviation of 0.071 in the case of respiration and a mean of 0.836 and a standard deviation of 0.035 in the case of breathhold data.

In conclusion, Fig. 1 suggests that ICA may be superior to CF for simultaneous EMG/MGG recordings in at least two respects, namely: 1) the agreement (amount of correlation) between the signals acquired using the two procedures and 2) the ability to minimize respiration artifacts from MGG data. This conclusion is supported by the contents of Fig. 2. This figure displays the same traces as in Fig. 1, though in a different manner that makes comparison easier from another perspective. Whereas Fig. 1 is useful to investigate the agreement between EMG and MGG (i.e., comparison of acquisition methods), Fig. 2 can be used to compare the artifact removal abilities of CF and ICA (i.e., comparison of signal processing methods).

In the top left section of Fig. 2, MGG raw data acquired during the breathhold (continuous trace, black color online) is presented against the CF-processed signal (dashed trace, red

color online) and the ICA-processed signal (dotted trace, blue color online). From this, it can be seen that CF and ICA yield qualitatively similar results for data acquired during breathholds. In the top right section of Fig. 2, MGG raw data acquired during respiration is compared to the CF and ICA signals using the same type of traces as in the previous example. In this case, however, it can be clearly seen that the respiration artifact is much larger in magnitude after CF than it is after ICA. The same situation was encountered in all ten datasets acquired. Finally, the bottom row traces of Fig. 2 display EMG raw and processed data acquired during the breathhold (bottom left) and during respiration (bottom right). This comparison is largely unremarkable, as both CF and ICA are found to perform very similarly for EMG signals. However, as pointed before, the main difference between the two methods lie in their unequal abilities to process MGG data, which clearly separates them from the standpoint of their utility.

In addition to signal waveform comparison between CF and ICA, we have also undertaken a frequency analysis comparison of the two methods. The motivation for this is the fact that, as explained in Section I, the frequency characteristics of EMG/MGG are important in distinguishing between healthy and diseased stomachs. Because of this, it is important to understand how CF and ICA are different in their ability to capture the information contained in the frequency characteristics of EMG/MGG signals. Fig. 3 displays a fast Fourier transform (FFT) frequency analysis of the same 1-min data segments presented in Figs. 1 and 2. The top left plot in Fig. 3 displays the frequency analysis of the raw data as acquired during respiration. Because the FFT method was used and the analyzed segment consisted of 1 min of data acquired at 200 Hz, false peaks exist due to harmonics present at integer multiples of the dominant frequency. For example, in the case of EMG, a false peak is clearly visible at approximately 6 cpm, though the true peak at 3 cpm evident of gastric activity is clearly superior in magnitude. The frequency analysis results for this segment after CF and ICA processing are shown in the same first column of Fig. 3 (middle left for CF and bottom left for ICA). Several conclusions can be drawn from inspecting these two plots. First, because of the filtering window used for CF and ICA before generating the FFT spectrum (1–30 cpm), the energy content due to low-frequency trends in the data is reduced in the CF and ICA plots (middle and bottom left), as distinct from the original raw data (top left). Second, a comparison of the CF and ICA plots for the breathhold segment leads to the conclusion that, as far as breathhold data are concerned, the frequency content of the analyzed signal is qualitatively the same whether the latter is analyzed using CF or ICA.

The results of our frequency analysis for the respiration signal are presented in the second column of Fig. 3. Comparing the ICA plot (bottom right) to the raw data plot (top right) shows that ICA has the ability to preserve the frequency peak due to gastric activity at the same frequency as in the original raw data, i.e., at 3 cpm. On the other hand, comparing the CF plot (middle right) to the original raw data plot (top right) shows that the CF method is not able to do this. Instead, the gastric frequency peak appears to be shifted to a frequency lower than the true frequency as determined from the raw data plot. Moreover, a large amount of energy is found, for the CF plot, in the neighborhood of the peak at 8 cpm. This is misleading because it suggests that the dominant frequency of the signal is in that region, which is not true because the raw data frequency analysis plot suggests otherwise. In conclusion, while the CF and ICA methods yield comparable frequency analysis results for breathhold data, ICA seems to be superior when respiration data are analyzed. On the other hand, as observed by an anonymous reviewer, although ICA is able to preserve the energy of the original data recorded during respiration better than CF does, the frequency of gastric activity is detected in a more precise manner using CF rather than ICA.

Fig. 4 displays the frequency waterfall plots of the entire datasets from which the waveforms discussed up to this point were selected. For this figure, each spectrum displayed was

created from a segment covering a period of 4 min, with an incremental step of 30 s for each successive spectrum. The first row displays CF-processed data and the second row displays ICA-processed data. Similarly, the first column displays MGG data while the second column displays EMG data. In the case of EMG, the results are very similar for CF and ICA. In the case of MGG, however, an important difference is that the height of the peak due to respiration (32 cpm) relative to the GI frequency content (1–10 cpm) is much higher for CF-processed data (top left) than it is for ICA-processed data (bottom left). This is true because in the case of the CF waterfall plot, the respiration peak "overshadows" the GI frequency content. In contrast to this, the ICA plot clearly demonstrates that the energy due to the respiration artifact is lower than that due to the GI content of the signal. This suggests that ICA is superior to the CF method from the standpoint of its ability to reduce respiration artifacts from MGG data.

Fig. 5 displays the same information as Fig. 4 but the frequency range displayed is 0–15 cpm as opposed to 0–40 cpm in Fig. 4. Whereas the purpose of Fig. 4 was to emphasize the respiration artifact content of each signal, that of Fig. 5 is to focus on the GI content of each spectrum. The conclusion to be drawn is that the two methods are largely similar from a qualitative standpoint regarding their ability to capture the frequency information of the original signal. For both MGG and EMG plots, the temporal evolution of the frequency components is loosely the same in the CF as in the ICA case. Though differences exist, their nature is predominantly quantitative rather than qualitative. However, as Fig. 3 suggests, ICA can sometimes be more trustworthy than the CF method for the purpose of frequency analysis though the reverse may occur in some cases. Nevertheless, as Fig. 5 shows, the two methods are comparable from this standpoint and qualitatively very similar.

It has long been known that the electric and magnetic GI signals are not stationary (see [3] and references therein). The stomach and intestine are positioned below the diaphragm, which implies that respiration artifacts can be strong. Moreover, the phenomenon of GI motility implies that the locations of the biological generators of recorded signals can shift during recording sessions. In two of our previous publications [3], [5], we discussed the extent to which ICA can be realistically used for the separation of gastric MGG and EMG signals. We demonstrated that, although ICA is capable of extracting the gastric MGG/EMG waveform, the large number of sources to which the recorded signals are due–as well as their large, motile spatial extent–can often severely undermine the task of ideally extracting the signals of interest from their recorded mixture. For this reason, it is often the case that ICA is more suitable for the *reduction* of large artifacts such as respiration and cardiac interference, rather than for the total *removal* of extraneous signals, which in our case can be significantly more difficult. Thus, what our present paper proposes is that ICA is often preferable to the use than CF for artifact reduction in MGG/EMG, even though the *complete* removal of such artifacts is not always practical.

Several important conclusions can be drawn from our comparison of CF and ICA for the analysis of simultaneous EMG/MGG signals. First, it was determined that the two methods yield very similar results for breathhold data. Second, ICA was found to be superior to the CF method in the case of segments acquired during respiration. Because the large majority of our datasets consist of such segments, our study indicates that ICA may be preferable to the CF method for the analysis of EMG/MGG signals. Third, it was found that, qualitatively, the two methods yield comparable results regarding their ability to capture the frequency information of the signals. In conclusion, our study suggests that ICA is the more reliable and trustworthy technique for the purpose of artifact reduction in EMG/MGG.

References

1. Cardoso JF. Blind signal separation: Statistical principles. Proc IEEE Oct;1998 86(10):2009–2025.
2. Hyvärinen A, Oja E. A fast fixed-point algorithm for independent component analysis. Neural Comput 1997;9:1483–1492.
3. Irimia A, Bradshaw LA. Artifact reduction in magnetogastrography using fast independent component analysis. Physiol Meas 2005;26:1059–1073. [PubMed: 16311453]
4. Irimia A. An integrative software package for gastrointestinal biomagnetic data acquisition and analysis using SQUID magnetometers. Comput Methods Programs Biomed 2006;83:83–94. [PubMed: 16857291]
5. Irimia, A.; Gallucci, MR.; Richards, WO.; Bradshaw, LA. Separation of gastric electrical control activity from simultaneous MGG/EGG recordings using independent component analysis. Proc 28th IEEE EMBS Annu Int Conf.; New York. Aug. 30–Sep. 3, 2006; p. 3110-3113.
6. Liang J, Chen JDZ. What can be measured from surface electrogastrography—Computer simulations. Dig Dis Sci 1997;42:1331–1343. [PubMed: 9246026]
7. Qian LW, Pasricha PJ, Chen JDZ. Origins and patterns of spontaneous and drug-induced canine gastric myoelectrical dysrhythmia. Dig Dis Sci 2003;48:508–515. [PubMed: 12757162]

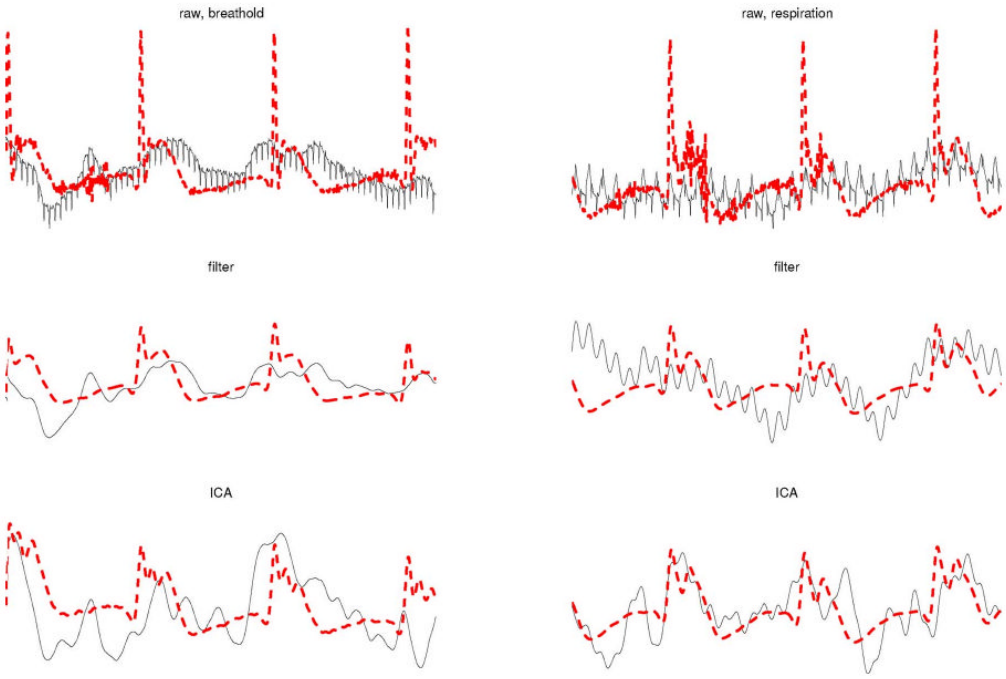

Fig. 1.

Validation across techniques of CF and ICA for artifact removal. MGG signals are shown as continuous (black color online) traces while EMG signals are shown as dashed (red color online) traces. The left column displays data acquired during a breathhold while the right column displays data acquired during respiration. The time interval shown is of 1 min in both cases. The first row displays raw data, the second row displays filtered data, and the third row displays ICA-processed data.

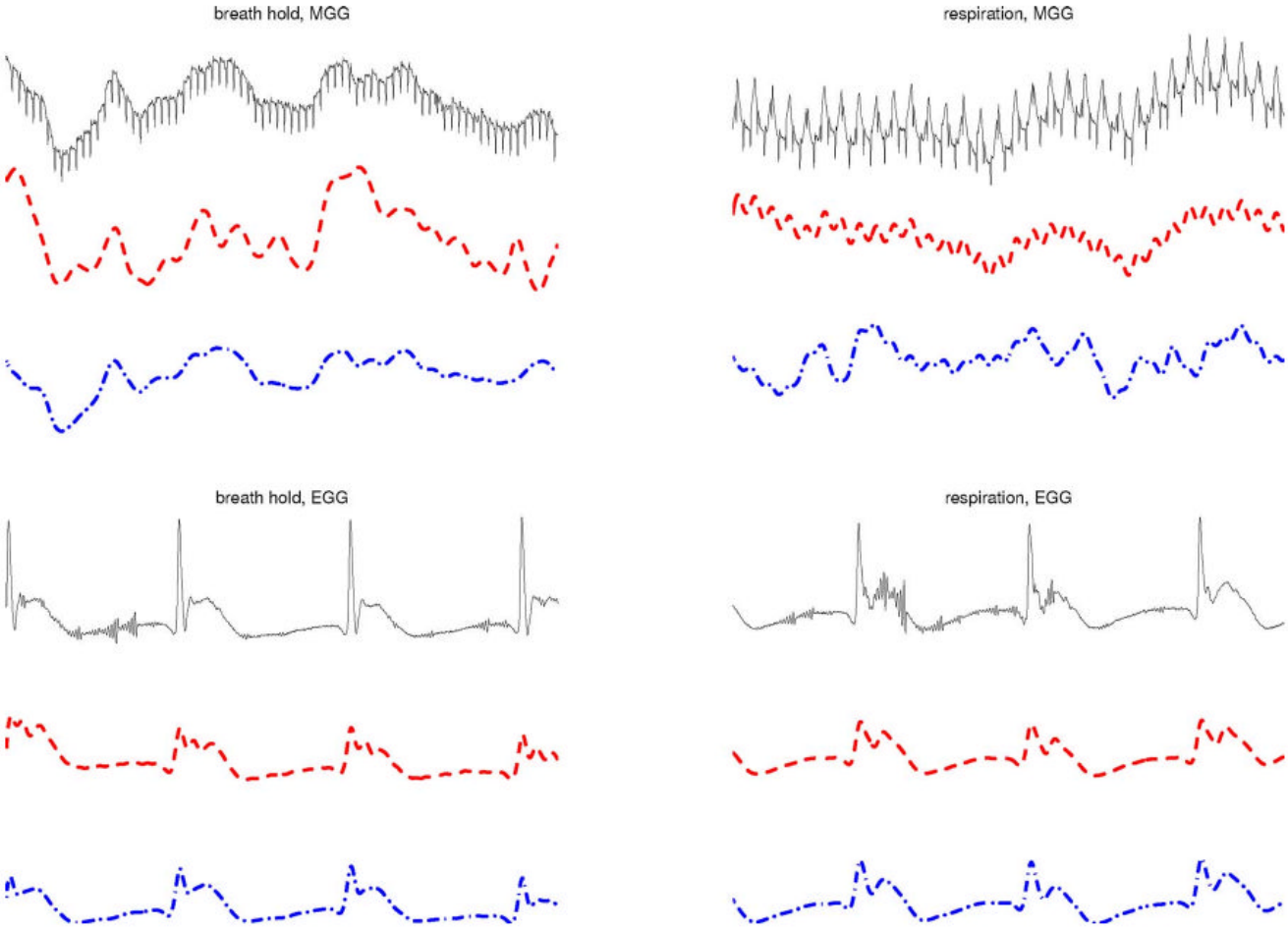

Fig. 2.

Comparison of CF and ICA for artifact removal in simultaneous EMG and MGG (II). Raw signals are shown as continuous (black color online, top) traces, filtered signals are shown as dashed (red color online, middle) traces, and ICA-processed signals are shown as dotted-dashed (blue color online, bottom) traces. The left column displays data acquired during a breathhold while the right column displays data acquired during respiration. The time interval shown is of 1 min in both cases. The first column displays MGG data while the second column displays EMG data.

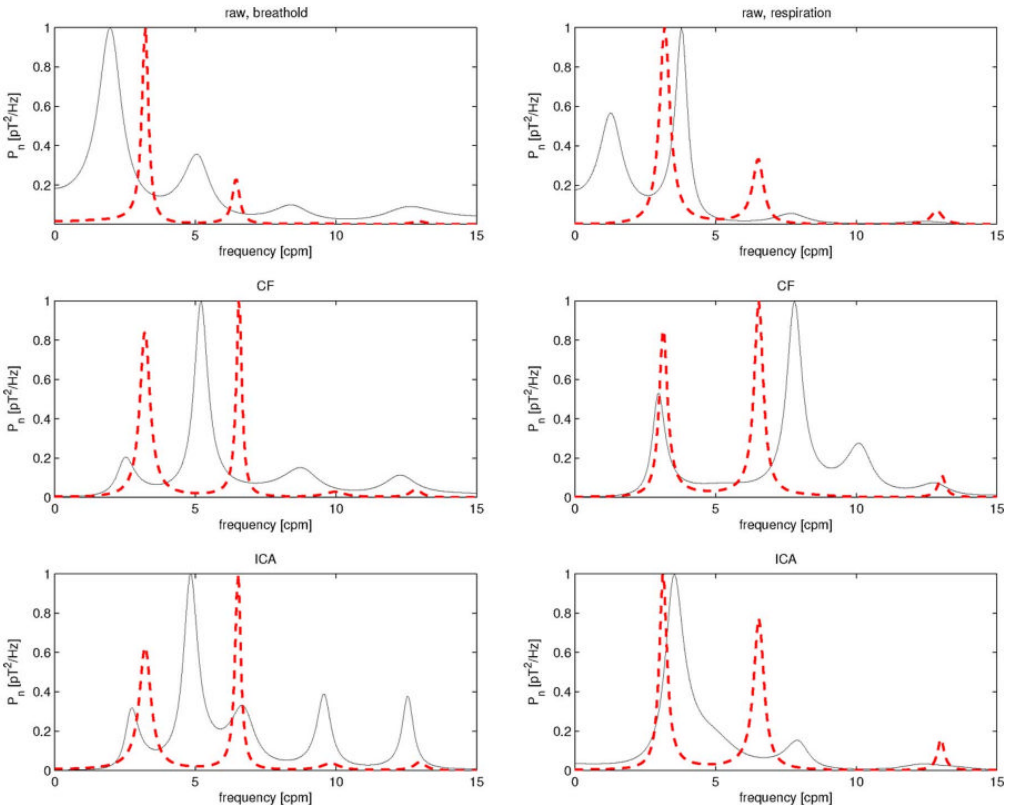

Fig. 3.

Frequency analysis results for the EMG/MGG data segments displayed in Figs. 1 and 2. MGG spectra are shown as continuous (black color online) traces while EMG spectra are shown as dashed (red color online) traces. The left column displays data acquired during a breathhold while the right column displays data acquired during respiration. The first row displays spectra for raw data, the second row displays spectra for filtered data, and the third row displays spectra for ICA-processed data. The units on the horizontal axis are hertz, while the vertical axis represents power displayed in units of picotesla squared per hertz. This figure demonstrates that, with regard to the frequency domain, CF and ICA perform comparably in identifying the dominant frequencies in the case of EMG. For MGG, however, ICA is clearly preferable for segments of data acquired during respiration, which is illustrated by the good agreement of the ICA MGG spectrum (third row, right) with the raw MGG spectrum (first row, right), whereas in the case of CF processing of MGG data (second row, right), there are false peaks that do not appear in the raw data spectrum.

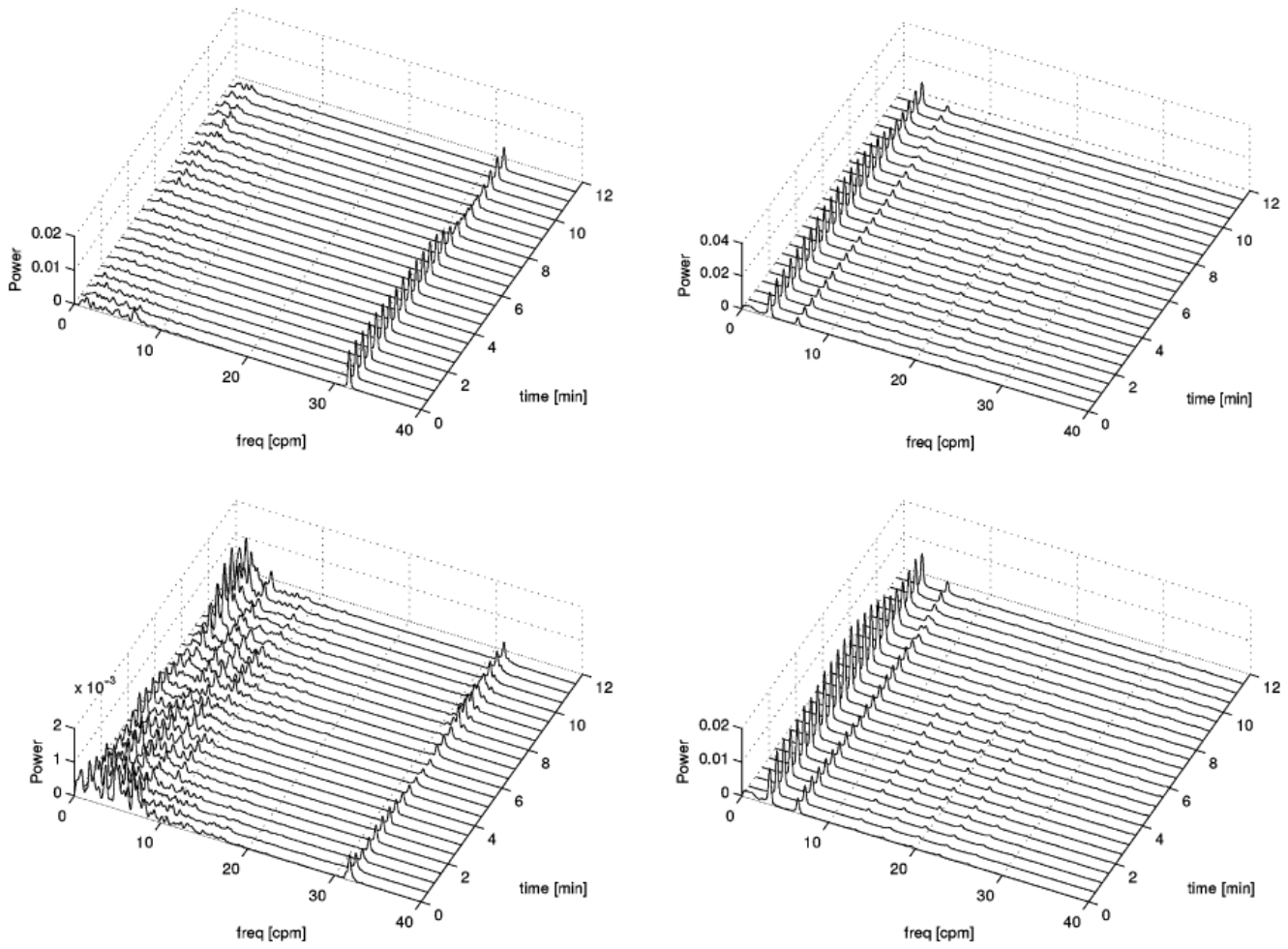

Fig. 4.

Comparison of waterfall plots for simultaneous EMG and MGG. The first columns displays MGG results and the second column displays EMG results. The first row refers to filtered data and the second row refers to ICA-processed data. The frequency range displayed is 0–40 cpm.

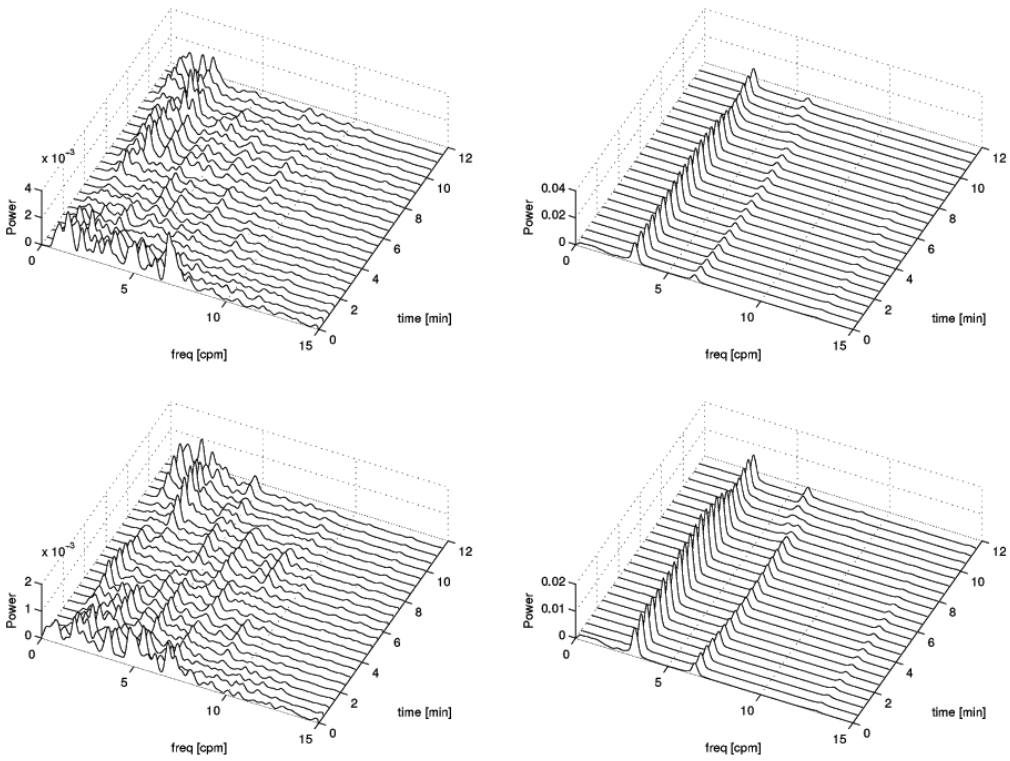

Fig. 5.
Same as Fig. 4, but with a frequency range displayed of 0–15 cpm.